Science Advances
AAAS

advances.sciencemag.org/cgi/content/full/5/7/eaav8192/DC1

Supplementary Materials for

Hippocampal theta phases organize the reactivation of large-scale electrophysiological representations during goal-directed navigation

Lukas Kunz*, Liang Wang, Daniel Lachner-Piza, Hui Zhang, Armin Brandt, Matthias Dümpelmann, Peter C. Reinacher, Volker A. Coenen, Dong Chen, Wen-Xu Wang, Wenjing Zhou, Shuli Liang, Philip Grewe, Christian G. Bien, Anne Bierbrauer, Tobias Navarro Schröder, Andreas Schulze-Bonhage, Nikolai Axmacher*

*Corresponding author. Email: lukas.kunz@uniklinik-freiburg.de (L.K.); nikolai.axmacher@rub.de (N.A.)

Published 3 July 2019, *Sci. Adv.* **5**, eaav8192 (2019)
DOI: 10.1126/sciadv.aav8192

This PDF file includes:

Supplementary Materials

Supplementary Tables

Table S1. Patient information.

Patient ID	Recording site	Age (y)	Sex	Handedness	Trial number	HC	PFC
1	Freiburg	37	M	R	160	Y	N
2	Freiburg	19	F	R	109	N	Y
3	Freiburg	45	F	A	51	Y	N
4	Freiburg	34	M	L	129	Y	N
5	Freiburg	59	M	R	40	Y	N
6	Freiburg	20	F	R	160	Y	N
7	Freiburg	28	F	R	160	Y	N
8	Bielefeld	35	F	L	100	N	N
9	Bielefeld	26	M	R	160	Y	Y
10	Beijing	25	M	R	91	Y	Y
11	Beijing	24	M	R	100	Y	Y
12	Beijing	23	M	R	115	Y	Y
13	Beijing	17	M	R	137	N	Y
14	Beijing	22	F	R	91	N	Y
15	Beijing	36	M	R	42	Y	N
16	Beijing	34	M	R	77	N	Y
17	Beijing	25	M	R	107	Y	Y
18	Beijing	22	F	R	86	N	Y
19	Beijing	27	F	R	49	Y	Y
20	Beijing	31	F	R	81	Y	Y
21	Beijing	19	F	R	79	Y	Y
22	Beijing	27	M	R	109	Y	N

F, female; M, male; R, right; L, left; A, ambidextrous; HC, at least one hippocampal channel available; PFC, at least one prefrontal channel available (assigned to either lateral orbitofrontal cortex or rostral middle frontal gyrus); Y, yes; N, no.

Table S2. MNI coordinates of hippocampal channels.

Patient ID	Hemisphere	MNI coordinates
1	L	-33/-15/-16
3	R	38/-15/-22
4	R	38/-18/-18
5	R	37/-10/-25
6	R	28/-7/-24
7	R	24/-15/-25
9	L	-25/-20/-15
10	L	-31/-31/-13
11	L	-31/-24/-13
12	R	33/-18/-16
15	L	-35/-22/-16
17	R	29/-18/-19
19	R	29/-16/-18
20	R	35/-22/-17
21	L	-30/-24/-13
22	L	-23/-5/-28

MNI, Montreal Neurological Institute; L, left; R, right.

Supplementary Figures

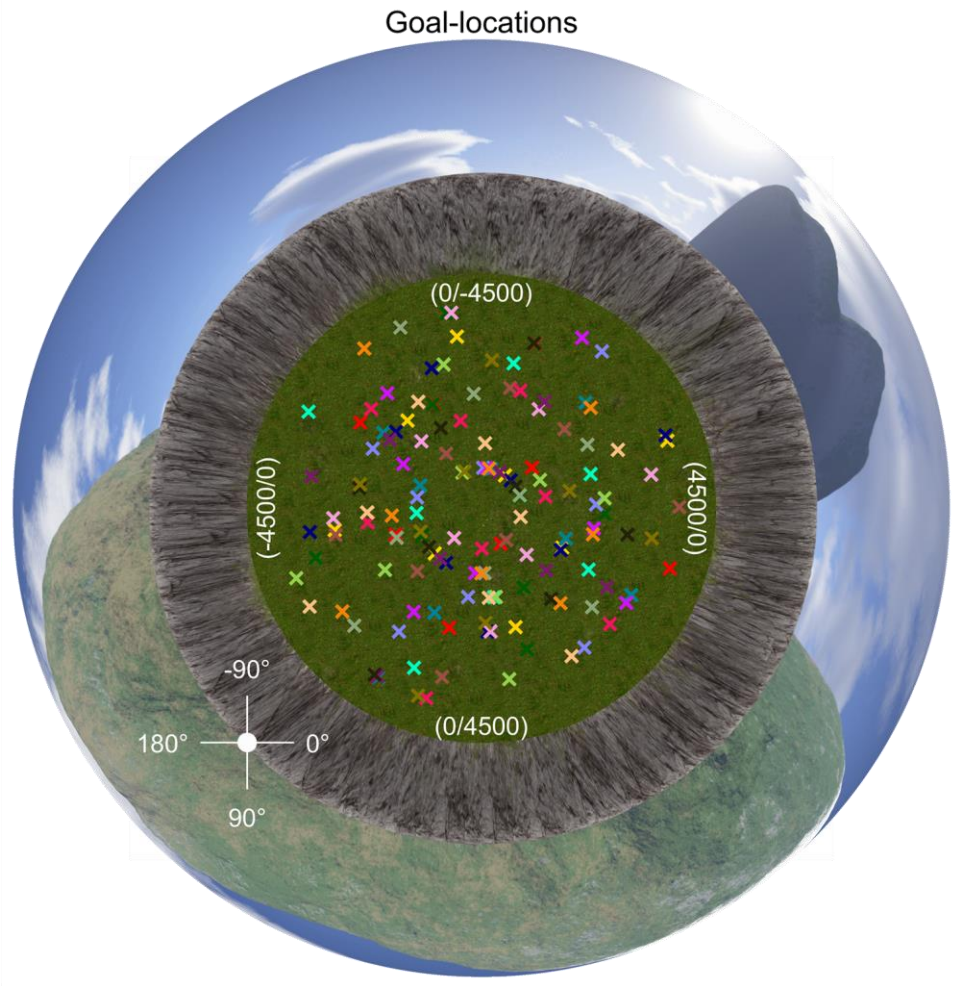

Fig. S1. Layout of the virtual environment and patient-wise goal locations. This figure shows the grassy plain from above, with a circular cliff surrounding the grassy plain. No intramaze landmarks are present. The entire background (including the mountains, the clouds, and the sun) is rendered at infinity. Please note that the y-axis is flipped upside down to combine the overhead view of the environment with the correct direction information when experiencing the virtual environment from the first-person perspective. Patient-wise correct goal-locations are indicated by colored crosses (one color per patient).

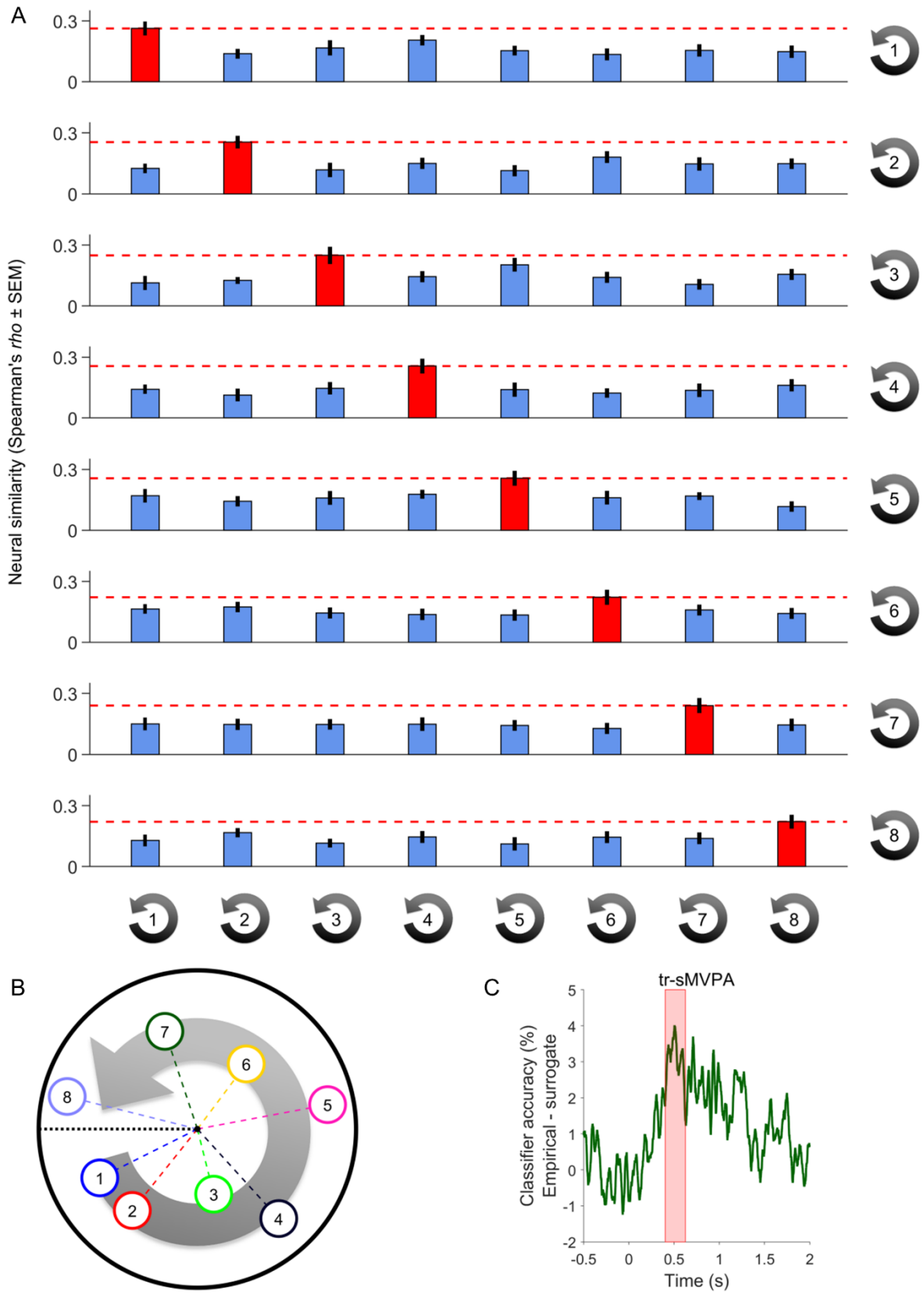

Fig. S2. Stimulus specificity of neural cue representations. (**A**) Average neural similarity values for identical cues from both data halves (red bars and red dotted lines) and for different cues from both data halves (blue bars). Correlations of neural representations from identical cues are consistently higher than correlations of neural representations from different cues. Cues are sorted by the angular orientation of the associated subjective goal-location within the virtual environment

(indicated by the ascending numbers within the black circular arrows). Error bars indicate standard error of the mean (SEM) across patients. (**B**) Conceptual depiction of the sorting procedure of the cues in (A). For each cue, the associated subjective goal-location is calculated (colored circles). The subjective goal-location of a given cue is the average response location of this cue. Subjective goal-locations are then sorted as a function of their relative locations within the virtual environment: For each cue, the angular orientation of the associated subjective goal-location in relation to a reference axis (dotted black line) is calculated (e.g., 51° for the red goal-location). Cues are then sorted as a function of angular orientation in ascending order (numbers within circles). (**C**) Time-resolved spatial multivariate pattern analysis (tr-sMVPA) using a linear *k*NN (*k*=10) classifier in combination with a 10fold cross-validation regime. The green line depicts dynamically changing classifier accuracy values (empirical classifier accuracy minus surrogate classifier accuracy). The red-shaded area indicates a significant difference between empirical classifier accuracy values and surrogate classifier accuracy values during a time period of 402-625ms after cue onset (cluster-based permutation testing, $t_{cluster}$ = 817.70, P = 0.001).

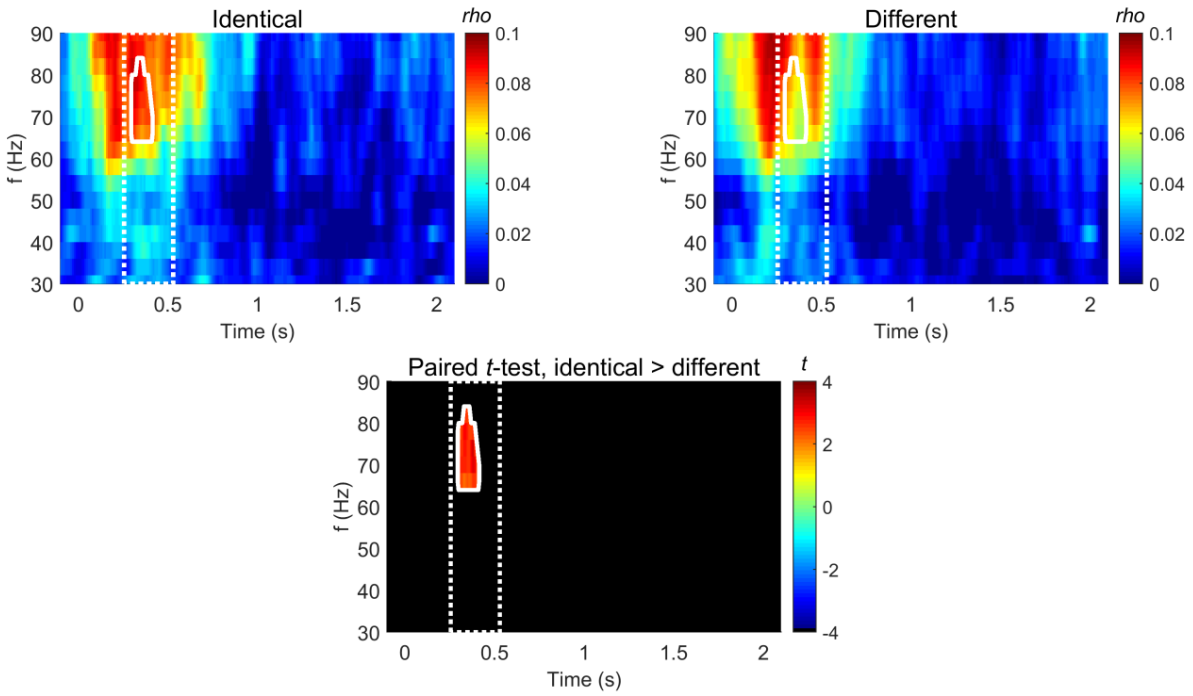

Fig. S3. Identification of large-scale electrophysiological cue representations using tr-sRSA based on gamma power. For each time-frequency bin, we obtained a measure of similarity between identical (upper left) and different (upper right) neural cue representations from both data halves (Spearman correlation). Both subplots show the average across patients. For each time-frequency bin, we then calculated a paired *t*-test between the similarity values from identical and different neural cue representations across patients (lower subplot; unsignificant time-frequency bins are masked out). Via cluster-based permutation testing, we identified a time-frequency area in which identical cue representations from both data halves exhibited significantly higher similarity values than different cue representations from both data halves (cluster-based permutation testing within the tROI resulting from the tr-sRSA of the time-domain data, $t_{cluster}$ = 125.24, P = 0.029). White line, significant cluster; white dotted line, tROI as defined by the significant time period in Fig. 2C; f, frequency; *t*, *t*-statistic from a paired *t*-test.

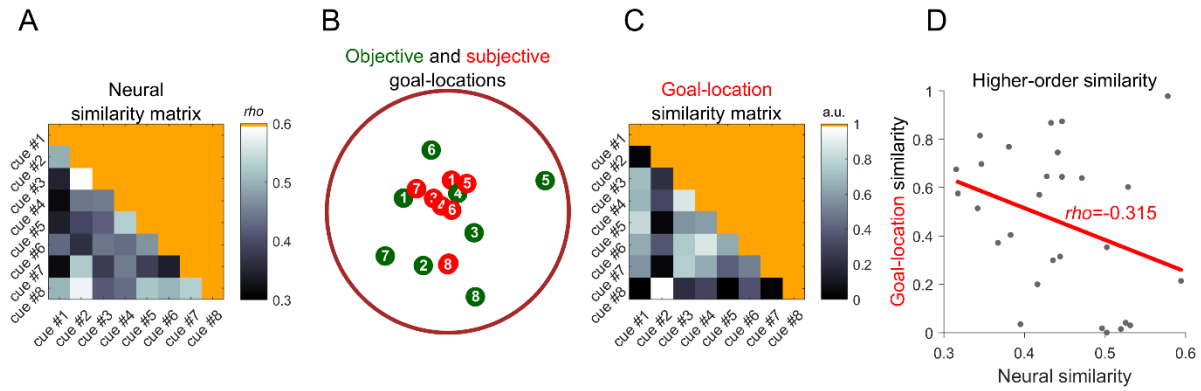

Fig. S4. Derivation of higher-order similarity. (**A**) For each pair of cues, we estimated the similarity of the associated neural cue representations (via nonparametric Spearman correlations). (**B**) Depiction of objective goal-locations (green) and subjective goal-locations (red). Subjective goal-locations were estimated as the average response location of each cue. (**C**) For each pair of cues, we estimated the Euclidean distance of the associated goal-locations and linearly converted this distance into a goal-location similarity value: goal-location similarity ($cues_{ij}$) = 1-D_{ij}/max(D), where D_{ij} is the Euclidean distance between the goal-locations of cue *i* and cue *j*. (**D**) To assess the higher-order similarity between the pair-wise similarity of neural cue representations and the pair-wise goal-location similarity, we calculated a Spearman correlation between both metrics, separately for each patient. The figure shows results from one patient. Resulting Spearman's *rho*-values were Fisher *z*-transformed and fed into a one-sample *t*-test across subjects to test for a consistent relationship between neural similarity matrices and goal-location similarity matrices. A similar statistical procedure was employed for all analyses of higher-order similarity (see *Inverse relationship between similarity of neural cue representations and similarity of associated subjective goal-locations*).

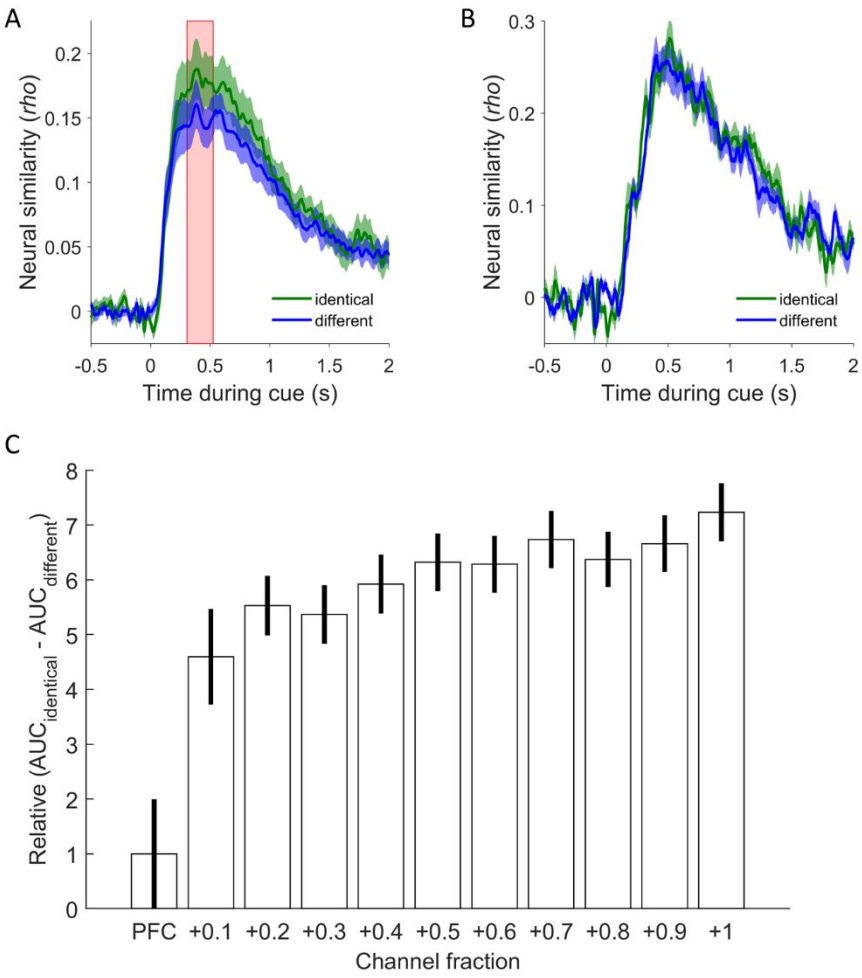

Fig. S5. Neural cue representations rely on large-scale electrophysiological signals. (**A**) Re-performing the tr-sRSA without channels located in lateral orbitofrontal cortex and rostral middle frontal gyrus still revealed higher neural similarity values for identical as compared to different cue representations between 305-525ms after cue onset (red shaded area; cluster-based permutation test, $t_{cluster}$ = 644.00, P = 0.027). (**B**) Re-performing the tr-sRSA only including channels located in lateral orbitofrontal cortex and rostral middle frontal gyrus did not lead to higher neural similarity values for identical as compared to different cues (cluster-based permutation testing, P = 0.400). (**C**) Largely stepwise increase in the difference between $AUC_{identical}$ (i.e., the area between neural similarity values of identical cues and the x-axis within the tROI) and $AUC_{different}$ (i.e., the area between neural similarity values of different cues and the x-axis within the tROI) when iteratively adding more channels to the tr-sRSA. The figure depicts values of ($AUC_{identical}$ - $AUC_{different}$) when adding 10% ("+0.1"), 20% ("+0.2"), …, or 100% ("+1") of other channels to the channels located in lateral orbitofrontal cortex or rostral middle frontal gyrus ("PFC"). Values are normalized with respect to the result in lateral orbitofrontal cortex and rostral middle frontal gyrus ("PFC") and thus termed "relative". Error bars depict standard error of the mean (SEM; again normalized with respect to the SEM of "PFC").

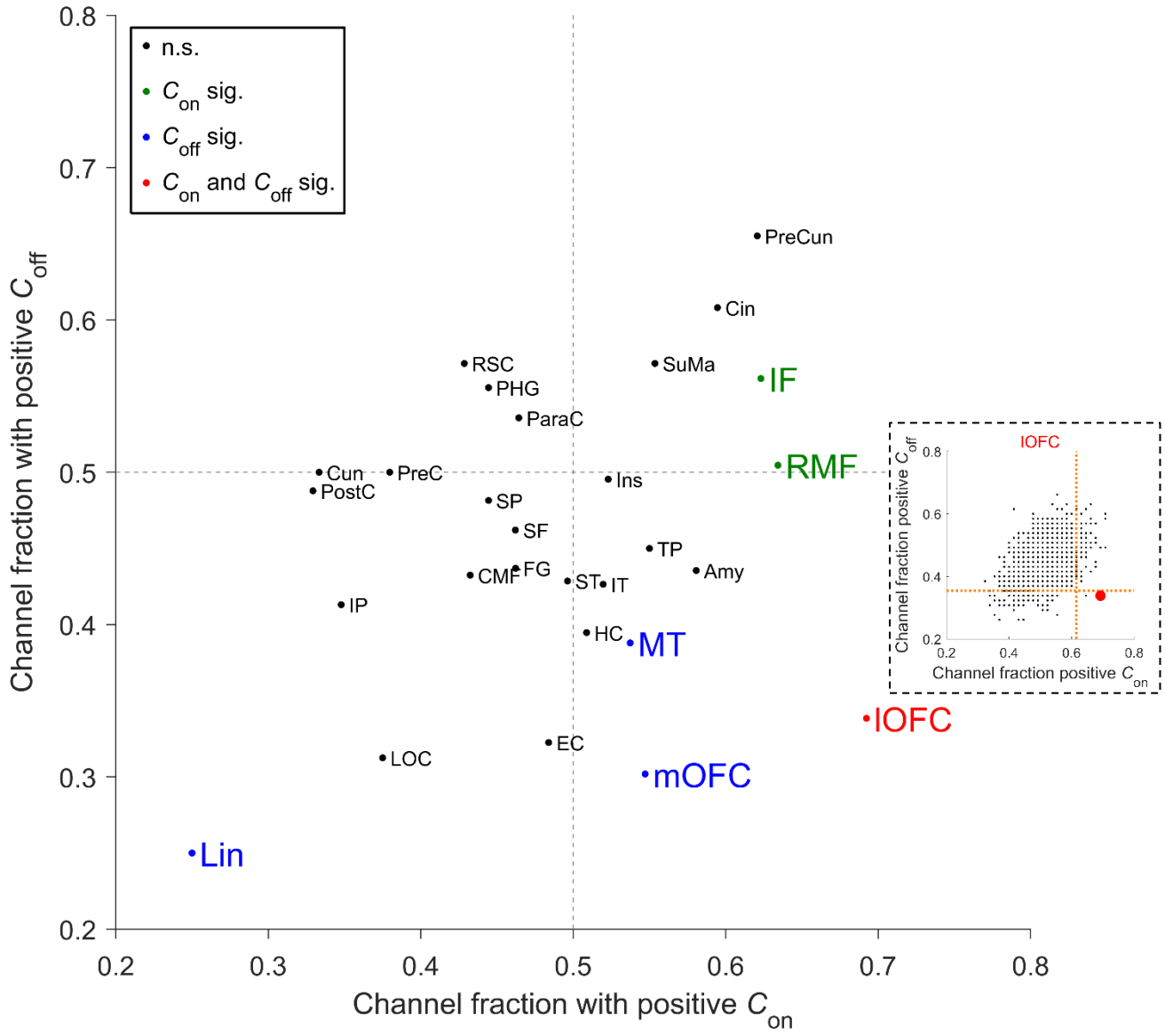

Fig. S6. Contribution of brain regions to the similarity of identical and different large-scale electrophysiological cue representations. Green, brain regions significantly increasing the similarity of identical cue representations (high fraction of channels with positive C_{on}; $P_{unc.} < 0.05$). Blue, brain regions significantly reducing the similarity of different cue representations (low fraction of channels with positive C_{off}; $P_{unc.} < 0.05$). Red, brain regions both significantly increasing the similarity of identical cue representations and significantly reducing the similarity of different cue representations ($P_{unc.} < 0.05$). Inset shows the statistical evaluation of the contribution of the lateral orbitofrontal cortex (lOFC) whose empirical channel fraction of positive C_{on}-values exceeds the 95th percentile of surrogate C_{on}-values (vertical dotted orange line) and whose empirical C_{off}-value falls below the 5th percentile of surrogate C_{off}-values (horizontal dotted orange line). Significance at an uncorrected alpha level of $P < 0.05$ (uncorrected for 29 regions) was determined using a region-wise permutation procedure (see *Materials and Methods*). Using Bonferroni correction for 29 regions to control for multiple comparisons, only lateral orbitofrontal cortex (lOFC) and rostral middle frontal gyrus (RMF) survived the statistical threshold regarding "channel fraction with positive C_{on}" (see also Fig. 2E; "channel fraction with positive C_{on}"-values are identical with "relative engagement"-values). No region survived Bonferroni correction for 29 regions when analyzing the "channel fraction with positive C_{off}". Amy, amygdala; CMF, caudal middle frontal gyrus; Cin, cingulate gyrus; Cun, cuneus;

EC, entorhinal cortex; FP, frontal pole; FG, fusiform gyrus; HC, hippocampus; IF, inferior frontal gyrus; IP, inferior parietal lobule; IT, inferior temporal gyrus; Ins, insula; LOC, lateral occipital cortex; lOFC, lateral orbitofrontal cortex; Lin, lingual gyrus; mOFC, medial orbitofrontal cortex; MT, middle temporal gyrus; ParaC, paracentral lobule; PHG, parahippocampal gyrus; PeCa, pericalcarine region (not shown since out of x- and y-limits; not significant); PostC, postcentral gyrus; PreC, precentral gyrus; PreCun, precuneus; RSC, retrosplenial cortex; RMF, rostral middle frontal gyrus; SF, superior frontal gyrus; SP, superior parietal lobule; ST, superior temporal gyrus; SuMa, supramarginal gyrus; TP, temporal pole; TT, transverse temporal gyrus. n.s., not significant; sig., significant at $P_{unc.} < 0.05$.

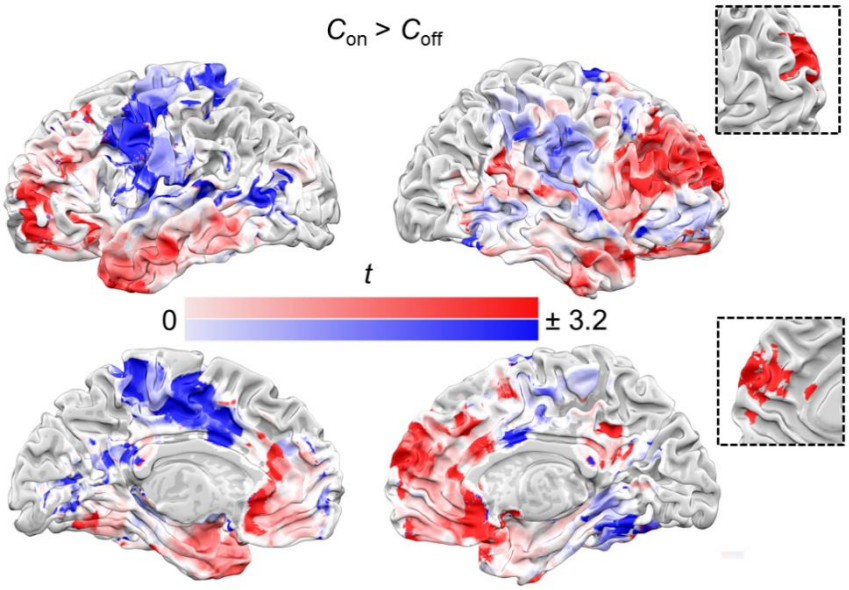

Fig. S7. Second-level statistics across patients depicting which brain regions simultaneously increased the neural similarity of identical cues and decreased the neural similarity of different cues. Brain regions in red both increase the neural similarity of identical cues and decrease the neural similarity of different cues, whereas blue regions both decrease the neural similarity of identical cues and increase the neural similarity of different cues (see also *Materials and Methods*). Inset shows the significant cluster in prefrontal cortex (cluster-based permutation testing, $P = 0.038$).

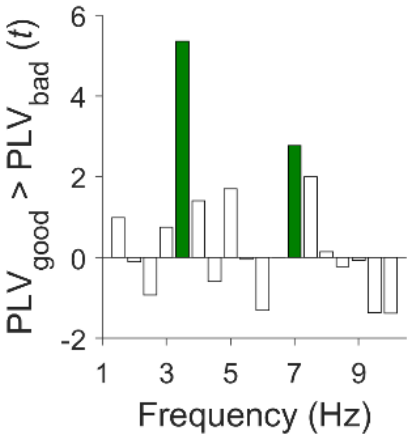

Fig. S8. Phase coupling (3.5 Hz) between the hippocampus and prefrontal cortex during goal-directed navigation. In a subset of *n*=8 patients with both hippocampal and prefrontal channels, we examined whether hippocampal-prefrontal phase coupling was enhanced for good versus bad trials during decision-making (last 1.5s of the retrieval period prior to participants' responses). Phase coupling was estimated via the phase locking value [PLV; (*33*)] across time, separately for each trial (*Materials and Methods*). We observed stronger phase coupling at 3.5Hz for good versus bad performance trials ($t(7) = 5.36$, $P = 0.019$, Bonferroni corrected for 18 frequencies). Control analyses showed that PLVs at 3.5Hz during good performance trials were also significantly higher than surrogate PLVs during good performance trials (paired *t*-test, $t(7) = 2.70$, $P = 0.030$), whereas PLVs at 3.5Hz during bad performance trials were not higher than surrogate PLVs during bad performance trials (paired *t*-test, $t(7) = -1.95$, $P = 0.092$). Green bars, $P_{unc.} < 0.05$.